Contribution from the Department of Chemistry,
The Ohio State University, Columbus, Ohio 43210

Phosphorus-31 NMR Studies and X-ray Structures of Five-Coordinate Cobalt(I) and Nickel(II) Complexes of Tris(2-(diphenylphosphino)ethyl)phosphine

William H. Hohman,† Dennis J. Kountz, and Devon W. Meek*

Received January 14, 1985

Two series of low-spin five-coordinate Co(I) and Ni(II) complexes of the tripod ligand tris(2-(diphenylphosphino)ethyl)phosphine, PP_3, were synthesized and characterized by elemental analyses, electronic absorption spectra, and $^{31}P\{^1H\}$ NMR spectra. The complexes have trigonal-bipyramidal geometries in which the PP_3 ligand occupies four of the five sites and a monodentate ligand occupies the fifth position. The ^{31}P NMR spectral patterns are consistent with AX_3 spin systems and trigonal-bipyramidal structures in solution. Several new complexes of the formulas $[Co(PP_3)(PR_3)]X$ and $[Ni(PP_3)(PR_3)]X_2$ were prepared. Generally, these pentaphosphorus complexes displayed first-order AMX_3 (occasionally second-order ABX_3) ^{31}P NMR splitting patterns at 36.43 MHz; they were studied to determine the effect of the fifth ligand on the chemical shift of the bridgehead phosphorus atom of PP_3. The complex $[Co(PP_3)(P(OMe)_3)]BF_4 \cdot 1.5H_2O$ crystallizes in the cubic space group $P\bar{4}3n$ with $a = 21.048$ (3) Å and $Z = 8$. The cation $[Co(PP_3)(P(OMe)_3)]^+$ (**1**) and the counterion BF_4^- lie on a crystallographic 3-fold axis. The isoelectronic complex $[Ni(PP_3)(P(OMe)_3)](AsF_6)_2 \cdot MeOH$ was also characterized by X-ray crystallography: $C_{46}H_{55}As_2F_{12}NiO_4P_5$ crystallizes in the monoclinic space group $P2_1/n$ with $a = 13.263$ (2) Å, $b = 19.929$ (5) Å, $c = 19.046$ (4) Å, $\beta = 96.15$ (1)°, and $Z = 4$. The cation $[Ni(PP_3)(P(OMe)_3)]^{2+}$ (**2**) and two AsF_6^- counterions lie in general crystallographic positions. Both the Co(I) and Ni(II) cations have similar structures, which are slightly distorted trigonal bipyramids; the most significant difference between the two geometries is the equatorial phosphorus to metal distances Co–P, 2.211 (6) Å, and Ni–P(av), 2.294 (2) Å.

Introduction

The syntheses and structural determinations of metal complexes of the potentially tetradentate tripod ligand tris(2-(diphenylphosphino)ethyl)phosphine (PP_3) continues to be a very active area of research.[1-6] Generally, PP_3 occupies four coordination positions around one metal ion to give a trigonal-bipyramidal structure; less commonly, PP_3 gives a square-pyramidal structure. In addition, there are examples in which PP_3 functions as a bi- or a tridentate ligand toward one metal and bridges to two or one other metal, respectively.[6] The different structural types for transition-metal complexes of tripodal phosphine and arsine ligands have been reviewed recently.[7,8]

Cobalt(I) and nickel(II) are isoelectronic d^8 ions that generally form low-spin, five-coordinate complexes with polyphosphine ligands. The $[CoL(PP_3)]$ and $[NiL(PP_3)]X$ (X = noncoordinating anion; L = a monodentate anionic ligand) complexes possess the trigonal-bipyramidal structure[9-13]

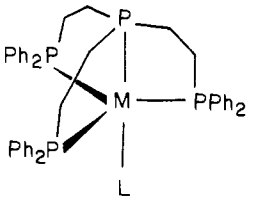

To date, few reports have appeared where L = a neutral PR_3 or $P(OR)_3$ ligand.[2] This paper reports the syntheses, characterizations, ^{31}P NMR spectra, and X-ray structural determinations of trigonal-bipyramidal PP_3 complexes of cobalt(I) and nickel(II) where L is a monodentate phosphorus ligand.

We have prepared two series of Co(I) and Ni(II) five-coordinate complexes of PP_3 in which the fifth ligand is varied. The ^{31}P NMR spectra of these complexes have been examined to correlate the phosphorus–phosphorus coupling constants and to determine the effect of the ligand L on the $^{31}P\{^1H\}$ NMR spectra of these trigonal-bipyramidal complexes. The structures of the complexes in solution are generally assigned by their electronic absorption spectra;[9,13a] in a few cases, X-ray crystal structures have been determined.[9,14] We report herein the X-ray crystal structures of the trimethyl phosphite complexes $[Co(PP_3)P(OMe)_3]BF_4 \cdot 1.5H_2O$ and $[Ni(PP_3)P(OMe)_3](AsF_6)_2 \cdot MeOH$.

Experimental Section

Reagents and Chemicals. The chemicals were reagent grade and they were used without further purification unless stated otherwise. Dimethylphenylphosphine, methoxydiphenylphosphine, triethylphosphine (distilled), and tris(2-(diphenylphosphino)ethyl)phosphine (PP_3) were purchased from Pressure Chemical Co. Triethyl phosphite, tris(2,2,2-trifluoroethyl) phosphite, and 2,2,2-trifluoroethanol were purchased from Aldrich Chemical Co. Trimethyl phosphite (Eastman Chemical Co.) was distilled from sodium under a nitrogen atmosphere. Methyldiisopropoxyphosphine[15] was furnished by Carolyn Supplee. The metal salts $Co(NCS)_2 \cdot 3H_2O$, $CoBr_2$, and $NiBr_2$ were obtained from City Chemical Corp., and $CoI_2 \cdot 2H_2O$ was obtained from Alfa Products. Organic solvents were purified by standard methods.

Instrumentation. Infrared spectra of the solid complexes were recorded on either a Perkin-Elmer 337 grating spectrophotometer (4000–400 cm^{-1}) or a Perkin-Elmer 283B grating spectrophotometer (4000–200 cm^{-1}) as KBr pellets and calibrated against the sharp 1601.4- and 906.7-cm^{-1} peaks of polystyrene film. The electronic spectra were recorded on a Varian 2300 vis/UV/near-IR spectrophotometer as CH_2Cl_2 solutions in quartz cuvettes. Several Co(I) compounds were run under N_2 pressure by evacuating the cuvettes and filling them via a syringe. Fourier-mode, proton-noise-decoupled ^{31}P NMR spectra were obtained on a Bruker HX-90 spectrometer operating at 36.43 MHz and equipped with a variable-temperature probe. The ^{31}P NMR spectra were obtained on CH_2Cl_2 solutions of the samples in 10-mm tubes using coaxial insert tubes containing the deuterium lock and trimethyl phosphate as a secondary standard ($\delta = 1.59$ relative to H_3PO_4). Positive chemical shifts

† Visiting Professor from Marietta College, Marietta, OH.

(1) Mealli, C.; Midollini, S.; Moneti, S.; Albright, T. A. *Helv. Chim. Acta* **1983**, *66*, 557.
(2) Cecconi, F.; Midollini, S.; Orlandini, A. *J. Chem. Soc., Dalton Trans.* **1983**, 2263.
(3) Gray, L. R.; Hale, A. L.; Levason, W.; McCullough, F. P.; Webster, M. *J. Chem. Soc., Dalton Trans.* **1984**, *47*.
(4) Cecconi, F.; Ghilardi, C. A.; Innocenti, P.; Mealli, C.; Midollini, S.; Orlandini, A. *Inrog. Chem.* **1984**, *23*, 922.
(5) Cecconi, F.; Ghilardi, C. A.; Midollini, S.; Moneti, S. *J. Chem. Soc., Dalton Trans.* **1983**, 349.
(6) Stoppioni, P.; Di Vaira, M.; Maitlis, P. M. *J. Chem. Soc., Dalton Trans.* **1982**, 1147.
(7) Mani, F.; Sacconi, L. *Comments Inorg. Chem.* **1983**, *2*, 157.
(8) Sacconi, L.; Mani, F. In "Transition Metal Chemistry"; Marcel Dekker: New York, 1982; Vol. 8, p 179.
(9) Ghilardi, C. A.; Midollini, S.; Sacconi, L. *Inorg. Chem.* **1975**, *14*, 1790.
(10) Sacconi, L.; Dapporto, P.; Stoppioni, P.; Innocenti, P.; Benelli, C. *Inorg. Chem.* **1977**, *16*, 1669.
(11) Stoppioni, P.; Dapporto, P.; Sacconi, L. *Inorg. Chem.* **1978**, *17*, 718.
(12) Orlandini, A.; Sacconi, L. *Inorg. Chem.* **1976**, *15*, 78.
(13) (a) King, R. B.; Kapoor, R. N.; Saran, M. S.; Kapoor, P. N. *Inorg. Chem.* **1971**, *10*, 1851. (b) King, R. B.; Cloyd, J. C. *Inorg. Chem.* **1975**, *14*, 1550.
(14) (a) Ghilardi, C. A.; Sacconi, L. *Cryst. Struct. Commun.* **1975**, *4*, 149. (b) Di Vaira, M.; Midollini, S.; Sacconi, L. *Cryst. Struct. Commun.* **1976**, *5*, 117.
(15) (a) Hoffman, F. W.; Moore, T. R. *J. Am. Chem. Soc.* **1958**, *80*, 2250. (b) Mastalerz, P. *Rocz. Chem.* **1964**, *38*, 61.

0020-1669/86/1325-0616$01.50/0

Table I. Analytical Data for the New $[Co(PP_3)(PR_3)]X$ and $[Ni(PP_3)(PR_3)]X_2$ Complexes[a]

complex	formula		% C	% H	% other
$[Co(PP_3)P(OMe)_3)]BF_4$	$C_{45}H_{51}BCoF_4O_3P_5$	calcd	57.47	5.47	16.47 (P)
		found	57.59	5.66	16.61
$[Co(PP_3)(PPh_2OMe)]AsF_6$	$C_{55}H_{55}AsCoF_6OP_5$	calcd	58.22	4.89	13.65 (P)
		found	58.43	5.00	13.83
$[Co(PP_3)(PEt_3)]AsF_6$	$C_{48}H_{57}AsCoF_6P_5$	calcd	55.61	5.54	14.94 (P)
		found	55.38	5.35	14.75
$[Co(PP_3)(PPhMe_2)]AsF_6$	$C_{50}H_{53}AsCoF_6P_5$	calcd	56.83	5.06	14.66 (P)
		found	56.64	4.92	14.89
$[Ni(PP_3)P(OMe)_3](AsF_6)_2$	$C_{45}H_{51}As_2F_{12}NiO_3P_5$	calcd	43.90	4.18	18.52 (F)
		found	43.74	4.19	19.71
$[Ni(PP_3)P(OEt)_3](AsF_6)_2$	$C_{48}H_{57}As_2F_{12}NiO_3P_5$	calcd	45.28	4.51	17.90 (F)
		found	45.12	4.66	18.08
$[Ni(PP_3)P(OCH_2CF_3)_3](BF_4)_2$	$C_{48}H_{48}B_2F_{17}NiO_3P_5$	calcd	46.83	3.93	26.23 (F)
		found	46.69	4.11	26.42

[a] Elemental analyses were performed by M-H-W Laboratories, Phoenix, AZ.

are downfield from the 85% H_3PO_4 standard. The ^{31}P NMR spectra were obtained on solutions of the complexes, protected from air, at low temperature to quench the effect of the nuclear quadrupole of cobalt and any fluxional tendencies of the cobalt or nickel complexes.

Syntheses of the Complexes. All manipulations were performed under an atmosphere of high-purity nitrogen using standard Schlenk techniques. Solvents were freshly distilled or purged with a N_2 stream for approximately 20 min immediately before use.

Syntheses of the $[CoL(PP_3)]$ Complexes ($L = Cl^-, Br^-, I^-, H^-, CN^-, NCS^-$). These compounds were prepared according to literature methods.[9]

Synthesis of $[Co(PP_3)CO]BF_4$. This compound was prepared by methods adapted from the preparation of $[Co(PR_3)_4CO]^+$, where PR_3 is a monodentate phosphine.[16a] A suspension of PP_3 (2.0 mmol) in 100 mL of isopropyl alcohol in a Pyrex Schlenk flask was saturated with carbon monoxide gas. To this magnetically stirred mixture was added $Co(BF_4)_2 \cdot 6H_2O$ (2.0 mmol). The solids dissolved to form an orange solution, and after several hours a yellow solid began to crystallize. Periodically, CO(g) was bubbled through the solution, and the mixture was stirred at room temperature for 24 h. The resultant yellow microcrystals were filtered, washed with *i*-PrOH and Et_2O, and dried in vacuo; yield 0.99 g (58%). The infrared carbonyl frequency of the solid, ν_{CO} = 1960 cm^{-1}, was identical with the reported value.[16b] The above compound could also be prepared by bubbling CO(g) through a mixture of $[CoBr(PP_3)]$ and NH_4BF_4 in isopropyl alcohol and then stirring the mixture under N_2 for 24 h.

Syntheses of the $[Co(PP_3)(PR_3)]AsF_6$ Complexes, Where PR_3 = PEt_3, $PPhMe_2$, PPh_2OMe, $P(OMe)_3$, and $PMe(O\text{-}i\text{-}Pr)_2$. A slight excess of monodentate phosphorus ligand was added via a syringe to a stirred mixture of $[CoL(PP_3)]$, where $L = Cl^-$, Br^-, and I^- (0.2 mmol) in 20 mL of methanol. To the dark green-brown slurry was added a slight excess of $LiAsF_6$ (>0.2 mmol). The color of the solution slowly changed from brown to red-violet, and the mixture was stirred overnight at room temperature. The resultant red or orange crystals were collected on a Schlenk frit, washed in sequence with MeOH, H_2O, MeOH, and Et_2O, and dried in vacuo. The complexes were isolated in 79%, 77%, 65%, 55%, and 51% yields, respectively. Elemental analyses of the first four complexes are given in Table I. The fifth compound contained a slight impurity, which proved to be difficult to remove. The infrared spectra of the solids showed peaks characteristic of the monodentate phosphorus ligand and the AsF_6^- anion, in addition to the PP_3 ligand absorptions.

Alternate Syntheses of $[Co(PP_3)P(OMe)_3]BF_4$. A slight excess of trimethyl phosphite (0.2 mmol) was added via a syringe to a solution of $[Co(PP_3)CO]BF_4$ (0.18 mmol) in 25 mL of methanol. The solution was irradiated (350-nm lamp) for 18 h while N_2 slowly swept over the stirring solution. The color of the solution changed from yellow to orange-red as a bright orange solid precipitated. The solid was collected on a frit, washed with MeOH and Et_2O, and dried in vacuo. More solid was obtained by evaporating the methanol filtrate to dryness; the solid was dissolved in CH_2Cl_2 (5 mL), and then methanol (6 mL) was added. As the CH_2Cl_2 solvent evaporated, more orange solid precipitated. The total yield was 0.10 g, 62%.

The above compound could also be prepared mixing equimolar amounts of $[Co(P(OMe)_3)_5]BF_4$ and PP_3 in methanol and then refluxing the solution. Evaporation of the methanol solvent produced an orange residue that was recrystallized from CH_2Cl_2 and methanol. The infrared spectra of the solid shows absorptions characteristic of both $P(OMe)_3$ and BF_4^-.

Syntheses of $[NiL(PP_3)]AsF_6$ Complexes, Where $L = Cl^-$, Br^-, and I^-. The preparation of these compounds was adapted from the literature preparation of $[NiCl(PP_3)]BPh_4$.[13a] One millimole of PP_3 was dissolved in 10 mL of CH_2Cl_2 and added to a solution of 1 mmol of NiL_2 and a slight excess of $LiAsF_6$ in 25 mL of EtOH. The solution turned from tan to red-purple. The mixture was heated at 50 °C for 1 h and then at reflux for 6 h; a dark purple solid formed. After the solvent was evaporated to half the original volume, the dark purple crystals were collected on a frit, washed with EtOH and Et_2O, and dried in vacuo.

A solution of NiI_2 was prepared by a metathesis reaction between KI and $Ni(NO_3)_2$ in EtOH. Solid KNO_3 was removed by filtration, and the resulting NiI_2 solution in EtOH was used for the synthesis of the iodide complex.

Synthesis of $[NiH(PP_3)]AsF_6$. This compound was prepared by the literature method.[9]

Synthesis of $[Ni(PP_3)CO](BF_4)_2$. This compound was prepared by the same method as $[Co(PP_3)CO]BF_4$ except that $Ni(BF_4)_2 \cdot 6H_2O$ was used. The orange compound was obtained in 68% yield; ν_{CO} = 2070 cm^{-1}.

Syntheses of $[Ni(PP_3)P(OMe)_3](AsF_6)_2$ and $[Ni(PP_3)P(OEt)_3](AsF_6)_2$. An excess of $P(OMe)_3$ or $P(OEt)_3$ was added via a syringe to a stirred mixture of $[NiBr(PP_3)]AsF_6$ (0.1 mmol) and a slight excess of $LiAsF_6$ (>0.1 mmol) in 10 mL of MeOH or EtOH, respectively. The color of the solution changed over a period of a few minutes from blue-purple to red-orange. An orange or orange-red solid started precipitating after approximately 10 min. After the mixtures were stirred for 2 h at room temperature, the respective solids were collected, washed with the corresponding alcohol and Et_2O, and then dried in vacuo. The two complexes were isolated in 45% and 77% yields. Elemental analyses are given in Table I. Attempts to prepare the corresponding $P(OCH_2CF_3)_3$ or PEt_3 derivative by this method were unsuccessful.

Synthesis of $[Ni(PP_3)P(OCH_2CF_3)_3](BF_4)_2$. A solution of PP_3 (0.3 mmol) in 20 mL of CH_2Cl_2 was added to a solution of $Ni(BF_4)_2 \cdot 6H_2O$ (0.3 mmol) in 10 mL of CF_3CH_2OH. A slight excess of $P(OCH_2CF_3)_3$ was added via a syringe to this solution. As the red-purple mixture was stirred, the color changed to a clear red solution; the solution then was heated to reflux (≃40 °C) for 2 h. Subsequently, the solution was stirred overnight at room temperature, and then a small amount of a tan solid was removed by filtration. Upon evaporation of 20 mL of the solvent mixture, 50 mL of Et_2O was added to the resulting blood red solution. The resultant dark red solid was collected on a frit and dried in vacuo; yield 66%. Elemental analyses are given in Table I. Phosphine derivatives of Ni(II) could not be isolated by this method.

X-ray Structural Determination of $[Co(PP_3)(P(OMe)_3)]BF_4 \cdot 1.5H_2O$ and $[Ni(PP_3)(P(OMe)_3)](AsF_6)_2 \cdot MeOH$. Translucent yellow-orange tetragonal prisms of $[Co(PP_3)(P(OMe)_3)]BF_4 \cdot 1.5H_2O$ and translucent orange prisms of $[Ni(PP_3)(P(OMe)_3)](AsF_6)_2 \cdot MeOH$ were grown over a period of 1 week by evaporation of the dichloromethane solutions. Preliminary room-temperature photographic work indicated that crystals of $[Co(PP_3)(P(OMe)_3)]BF_4 \cdot 1.5H_2O$ (**1**) possessed a cubic unit cell with systematic absences *hhl* ($l = 2n + 1$) and $Z = 8$, and crystals of $[Ni(PP_3)(P(OMe)_3)](AsF_6)_2 \cdot MeOH$ (**2**) belonged to the monoclinic space group C_{2h}^5-$P2_1/n$ (alternative setting of $P2_1/c$, No. 14), $Z = 4$.

Intensity data were collected at 153 and 155 K for **1** and **2**, respectively, on a Syntex $P\bar{1}$ diffractometer equipped with a LT-1 low-temperature device. Data collection and data reduction followed the standard practice at The Ohio State University.[17] Table II provides crystallo-

(16) (a) Rigo, P.; Bressan, M.; Morvillo, A. *J. Organomet. Chem.* **1976**, *105*, 263. (b) Peterson, R. L.; Watters, K. L. *Inorg. Chem.* **1973**, *12*, 3009.

Table II. Crystallographic Details for $[Co(PP_3)(P(OMe)_3)]BF_4 \cdot 1.5H_2O$ (**1**) and $[Ni(PP_3)(P(OMe)_3)](AsF_6)_2 \cdot MeOH$ (**2**)

	$C_{45}H_{54}BCoF_4O_{4.5}P_5$	$C_{46}H_{55}As_2F_{12}NiO_4P_5$
fw	967.55	1232.36
space group	T_d^4–$P\bar{4}3n$	C_{2h}^5–$P2_1/n$
a, Å	21.048 (3)	13.263 (2)
b, Å		19.929 (5)
c, Å		19.046 (4)
β, deg		96.15 (1)
V, Å^3	9324.6 (5)	5005 (2)
Z	8	4
ρ_c, g/cm^3	1.38[a]	1.64[b]
ρ_o, g/cm^3	1.39[c]	1.63[c]
linear abs coeff, cm^{-1}	5.6	22.8
transmission coeff[d]	0.842–0.911	0.376–0.735
cryst size, mm	0.17 × 0.35 × 0.38	0.15 × 0.49 × 1.03
bounding cryst faces	{100}, {010}, {001}	{100}, {010}, {001}, {$\bar{1}\bar{1}\bar{1}$}
temp, K	153	155
radiation	graphite-monochromated Mo Kα (λ(Kα_1) = 0.709 26 Å)	same
collcn range	$\pm h,\pm k,+l$	$\pm h,+k,+l$
2θ limits, deg	$4.0 \leq 2\theta \leq 55.0$	$4.0 \leq 2\theta \leq 56.0$
scan type	ω–2θ	same
scan width, deg	0.9 below Kα_1 to 1.0 above Kα_2	1.0 below Kα_1 to 1.2 above Kα_2
scan speed, deg/min	4.0–24.0	same
bkgd time/scan time	0.5	same
no. of reflcns measd	7000	13 691
no. of unique data with $F_o^2 \geq 3\sigma(F_o^2)$	1204	7210
no. of variables	86	353
$R(F)$[e]	0.108	0.062
$R_w(F)$[f]	0.101	0.063

[a] Calculated at 153 K. [b] Calculated at 155 K. [c] Measured by buoyancy method at 298 K. [d] Analytical absorption correction was applied. [e] $R = \sum(|F_o| - |F_c|)/\sum|F_o|$. [f] $R_w = [\sum w(|F_o| - |F_c|)^2/\sum w|F_o|^2]^{1/2}$. The function minimized during least squares is $\sum w(|F_o| - |F_c|)^2$, where $w = 1/\sigma^2(F_o)$.

graphic and data collection details. Six reflections measured every 100 reflections during data collection revealed minor crystal deterioration; both data sets were corrected for small decay rates and for absorption. Atomic scattering factors for the non-hydrogen[18] and hydrogen[19] atoms were from the standard sources. Anomalous dispersion corrections for the nonhydrogen atoms were included as $\Delta f'$ and $\Delta f''$ terms.[18] Data reduction was performed by using the CRYM programs[20] and all least-squares refinements were done with SHELX-76.[21]

Two choices of cubic space group, T_d^4–$P\bar{4}3n$ (No. 218) and O_h^3–$Pm3n$ (No. 223), were consistent with the systematic absences and $m3m$ Laue symmetry for **1**. A Patterson map could be interpreted self-consistently only in space group $P\bar{4}3n$ with the cobalt atom on a crystallographic 3-fold axis. The cobalt atom position was used in the DIRDIF program[22] to locate all the remaining nonhydrogen atoms.

Table III. Fractional Coordinates (×10^4) for $[Co(PP_3)(P(OMe)_3)]BF_4 \cdot 1.5H_2O$

atom	x	y	z	B,[a] Å^2
Co	−1692.5 (13)	−1692.5 (13)	−1692.5 (13)	1.71 (8)
P1	−1048 (3)	−1404 (3)	−2470 (3)	1.9 (3)
P2	−1109 (3)	−1109 (3)	−1109 (3)	2.0 (3)
P3	−2270 (3)	−2270 (3)	−2270 (3)	1.7 (3)
C1	−329 (9)	−960 (11)	−2140 (9)	3.2 (5)
C2	−494 (9)	−634 (9)	−1573 (10)	2.5 (5)
O1	−2224 (6)	−2141 (6)	−3042 (6)	2.3 (10)
CO1	−2280 (11)	−2598 (11)	−3565 (10)	5.5 (25)
C111	−1350 (6)	−826 (6)	−3065 (6)	1.4 (5)
C112	−1556 (6)	−1026 (6)	−3661 (6)	1.8 (5)
C113	−1760 (6)	−581 (6)	−4108 (6)	2.5 (5)
C114	−1755 (6)	65 (6)	−3959 (6)	3.8 (5)
C115	−1547 (6)	265 (6)	−3362 (6)	3.5 (6)
C116	−1344 (6)	−180 (6)	−2915 (6)	2.0 (6)
C121	−642 (6)	−1964 (6)	−2949 (6)	1.4 (5)
C122	−741 (6)	−2615 (6)	−2874 (6)	2.8 (5)
C123	−409 (6)	−3047 (6)	−3252 (6)	3.2 (5)
C124	21 (6)	−2827 (6)	−3706 (6)	2.8 (5)
C125	120 (6)	−2176 (6)	−3781 (6)	2.4 (5)
C126	−212 (6)	−1745 (6)	−3403 (6)	3.7 (5)
B	1263 (14)	1263 (14)	1263 (14)	2.0 (12)
F1	854 (7)	854 (7)	854 (7)	4.1 (7)
F2	935 (5)	1812 (6)	1284 (5)	2.7 (8)
		Solvent		
O2	0	659 (7)	−5000	1.0 (4)

[a] Equivalent isotropic thermal parameters calculated from the anisotropic thermal tensor for atoms with anisotropic thermal parameters.

Full-matrix least-squares refinement (without anomalous scattering contributions) was performed with the phenyl rings treated as rigid hexagons (D_{6h} symmetry with d_{C-C} = 1.395 Å). After convergence of this model, the anomalous dispersion corrections were included in further isotropic refinements of two models: the (x, y, z) enantiomorph refined to R = 0.119 and R_w = 0.120; the $(\bar{x}, \bar{y}, \bar{z})$ enantiomorph, obtained by reversing the signs of all atomic coordinates, refined to values of R = 0.118 and R_w = 0.119. A comparison of these results slightly favors the $(\bar{x}, \bar{y}, \bar{z})$ enantiomorph.[23] The methyl hydrogen atoms were then found in a difference electron density map, and the remaining hydrogen atoms were fixed at calculated positions (d_{C-H} = 0.95 Å, $B(H) = B_{iso}(C) + 1.0$ Å^2).

During the final cycles of full-matrix least-squares refinement the non-hydrogen atoms, except for the phenyl and methylene carbon atoms, were converted to anisotropic thermal refinement. The three highest peaks in the difference electron density map were found on crystallographic 2-fold axes at $(x, {}^1/_2, 0)$ and $(x, 0, 0)$ and at a general position; these were presumed to be oxygen atoms from water molecules. Only the oxygen atoms at $(x, {}^1/_2, 0)$ refined; the solvent molecules appear highly disordered in the lattice. The final $R(F_o)$ = 0.108 and $R_w(F_o)$ = 0.101 for 1204 reflections with $F_o^2 \geq 3\sigma(F_o)$ and 86 variables. The largest peak (2.5 e/Å^3) in the difference electron density map is near the solvent molecule; additional peaks (1.5 e/Å^3 and 2.2 e/Å^3) in the difference map occurred between the cobalt and phosphorus atoms on the crystallographic 3-fold axis and may be partially the result of concentration of errors in the electron density map at special positions.[24] Final values for the atomic parameters are given in Table III; bond lengths and angles are listed in Tables V and VI.

MULTAN80[25] was used to find two arsenic atoms, one nickel, and five phosphorus atoms in $[Ni(PP_3)(P(OMe)_3)](AsF_6)_2 \cdot MeOH$. The remaining non-hydrogen atoms were located by standard Fourier techniques. For each disordered AsF_6^- anion, 12 distinct peaks were found for the fluorine atoms corresponding to two interpenetrating approximate octahedra for each anion; partial occupancies of the two orientations for each anion were refined.

A methanol solvent molecule was found disordered across the inversion center at the origin in the difference electron density map; again, partial occupancies of two superimposed orientations were refined. The methyl

(17) Christoph, G. G.; Engel, P.; Usha, R.; Balogh, D. W.; Paquette, L. A. *J. Am. Chem. Soc.* **1982**, *104*, 784. Scan counts were transformed to integrated intensities by using the formula $I = R(C - T(B_1 + B_2))$, where R is the scan rate, C is the number of scan counts, T is the ratio of the total scan time to the background counting time, and B_1 and B_2 are the measured background at each end of the scan. Estimated standard deviations were calculated as $\sigma^2(I) = R^2(C + T^2(B_1 + B_2) + (pI)^2)$, where p = 0.02 is the coefficient for errors expected proportional to the diffracted intensity. Intensities were reduced to $|F_o|$ after applying Lorentz and polarization corrections: $|F_o| = (I/Lp)^{1/2}$ and $\sigma(F_o) = \sigma(I)/2(Lp)^{1/2}$.

(18) Cromer, D. T.; Weber, J. T. "International Tables for X-ray Crystallography"; Kynoch Press: Birmingham, England, 1974; Vol. IV, p 71.

(19) Stewart, R. F.; Davidson, E. R.; Simpson, W. T. *J. Chem. Phys.* **1965**, *42*, 3175.

(20) DuChamp, D. J. "CRYM", "Program and Abstracts", American Crystallographic Association Meeting, Bozeman, MT, 1965; Paper 13–14.

(21) Sheldrick, G. M. "SHELX-76. A Program for Crystal Structure Determination", University Chemical Laboratory, Cambridge, England, 1976.

(22) Beurskens, P. T.; Bosman, W. P.; Doesburg, H. M.; Gould, R. O.; Van den Hark, T. E. M.; Prick, P. A. J.; Noordik, J. H.; Beurskens, G.; Parthasarthi, V.; Haltiwanger, R. C.; Bruins Slot, H. J. "DIRDIF: Application of Direct Methods for Difference Structures"; University of Nijmegen, Nijmegen, The Netherlands, 1983.

(23) Bijvoet, J. M.; Peerdeman, A. F.; van Bommel, A. J. *Nature* (London) **1951**, *168*, 271.

(24) De Wolff, P. M. *Acta Crystallogr.* **1966**, *20*, 141.

(25) Main, P.; Fiske, S. J.; Hull, S. E.; Lessinger, L.; Germain, G.; Declercq, J.-P.; Woolfson, M. M. "MULTAN80: A System of Computer Programmes for the Automatic Solution of Crystal Structures from X-Ray Diffraction Data", University of York, England, and University of Louvain, Belgium, 1980.

Table IV. Fractional Coordinates ($\times 10^4$) for $[Ni(PP_3)(P(OMe)_3)](AsF_6)_2 \cdot MeOH$

atom	x	y	z	B,[a] Å^2	atom	x	y	z	B,[a] Å^2	pop.[b]
Ni	−7039.3 (6)	−2953.3 (4)	−5998.4 (4)	1.40 (3)	C312	−7320 (3)	−3130 (2)	−8214 (2)	1.8 (1)	
P1	−5966.1 (12)	−2266.4 (8)	−5320.4 (9)	1.63 (7)	C313	−7802 (3)	−3265 (2)	−8887 (2)	2.1 (1)	
P11	−8549.5 (12)	−3311.0 (8)	−5660.1 (9)	1.60 (7)	C314	−7873 (3)	−3923 (2)	−9136 (2)	2.5 (1)	
P111	−6398.7 (13)	−3757.8 (8)	−5313.2 (9)	1.66 (7)	C315	−7462 (3)	−4447 (2)	−8712 (2)	2.5 (2)	
P2	−6278.8 (12)	−3480.7 (8)	−6894.7 (9)	1.50 (7)	C316	−6980 (3)	−4313 (2)	−8039 (2)	2.2 (2)	
P3	−7762.0 (13)	−2167.5 (8)	−6628.8 (9)	1.71 (7)	C321	−5068 (2)	−3122 (2)	−7097 (2)	2.0 (1)	
O1	−7148 (4)	−1839 (2)	−7194 (2)	3.2 (2)	C322	−4148 (2)	−3385 (2)	−6794 (2)	2.3 (2)	
O2	−8089 (4)	−1566 (2)	−6168 (2)	2.7 (2)	C323	−3236 (2)	−3097 (2)	−6943 (2)	3.3 (2)	
O3	−8717 (3)	−2457 (2)	−7079 (2)	2.3 (2)	C324	−3244 (2)	−2546 (2)	−7395 (2)	3.3 (2)	
CO1	−6780 (6)	−1178 (4)	−7257 (4)	3.1 (2)	C325	−4164 (2)	−2283 (2)	−7698 (2)	2.8 (2)	
CO2	−8921 (6)	−1133 (4)	−6342 (4)	4.3 (2)	C326	−5076 (2)	−2571 (2)	−7550 (2)	2.3 (2)	
CO3	−9302 (6)	−2150 (4)	−7678 (4)	3.6 (2)	As1	−8512.0 (5)	520.9 (4)	−2279.0 (4)	2.34 (3)	
C1	−4992 (5)	−2827 (3)	−4892 (4)	2.0 (3)	F11A	−8732 (7)	1067 (6)	−2969 (6)	4.2 (2)	0.55 (2)
C2	−5561 (5)	−3411 (3)	−4588 (3)	2.0 (3)	F12A	−8411 (7)	−33 (5)	−1580 (5)	3.3 (2)	0.55 (2)
C11	−8226 (5)	−3756 (3)	−4821 (3)	2.1 (3)	F13A	−9450 (9)	125 (6)	−2759 (5)	4.9 (2)	0.55 (2)
C12	−7377 (5)	−4239 (3)	−4946 (3)	1.9 (3)	F14A	−9332 (10)	770 (6)	−1725 (7)	6.1 (3)	0.55 (2)
C31	−5977 (5)	−4327 (3)	−6558 (3)	1.7 (3)	F15A	−7496 (10)	940 (5)	−1791 (5)	4.5 (2)	0.55 (2)
C32	−5618 (5)	−4326 (3)	−5774 (3)	2.0 (3)	F16A	−7623 (10)	293 (7)	−2819 (8)	6.6 (3)	0.55 (2)
C111	−5240 (3)	−1583 (2)	−5655 (2)	1.6 (1)	F11B	−8740 (10)	1259 (7)	−2741 (8)	4.6 (3)	0.45
C112	−5552 (3)	−921 (2)	−5581 (2)	2.0 (1)	F12B	−8125 (11)	−167 (7)	−1794 (8)	5.4 (4)	0.45
C113	−4987 (3)	−396 (2)	−5825 (2)	2.3 (2)	F13B	−9175 (9)	−110 (7)	−2779 (6)	3.3 (2)	0.45
C114	−4110 (3)	−534 (2)	−6143 (2)	2.6 (2)	F14B	−9710 (11)	741 (6)	−1996 (8)	4.6 (3)	0.45
C115	−3798 (3)	−1196 (2)	−6217 (2)	2.5 (2)	F15B	−7941 (11)	1131 (6)	−1757 (6)	3.6 (3)	0.45
C116	−4363 (3)	−1721 (2)	−5973 (2)	2.3 (2)	F16B	−7433 (11)	266 (7)	−2555 (9)	4.9 (4)	0.45
C121	−6440 (3)	−1868 (2)	−4563 (2)	1.9 (1)	As2	−2382.1 (5)	−3834.6 (3)	−4405.1 (4)	2.14 (3)	
C122	−7481 (3)	−1799 (2)	−4531 (2)	2.9 (2)	F21A	−3372 (11)	−4196 (7)	−4902 (7)	2.8 (3)	0.58 (4)
C123	−7837 (3)	−1486 (2)	−3951 (2)	8.1 (2)	F22A	−1424 (9)	−3440 (6)	−3866 (7)	3.2 (2)	0.58 (4)
C124	−7152 (3)	−1242 (2)	−3403 (2)	3.6 (2)	F23A	−2246 (11)	−4505 (5)	−3850 (6)	2.4 (2)	0.58 (4)
C125	−6112 (3)	−1311 (2)	−3435 (2)	3.1 (2)	F24A	−3063 (12)	−3379 (6)	−3896 (6)	3.2 (2)	0.58 (4)
C126	−5756 (3)	−1625 (2)	−4016 (2)	2.8 (2)	F25A	−2622 (13)	−3151 (5)	−4969 (5)	2.8 (2)	0.58 (4)
C211	−9599 (3)	−2769 (2)	−5484 (2)	1.9 (1)	F26A	−1706 (11)	−4238 (6)	−4993 (9)	4.3 (2)	0.58 (4)
C212	−10326 (3)	−2601 (2)	−6040 (2)	2.4 (2)	F21B	−3517 (14)	−4196 (9)	−4809 (10)	2.5 (4)	0.42
C213	−11127 (3)	−2176 (2)	−5922 (2)	2.8 (2)	F22B	−1271 (16)	−3545 (10)	−4014 (12)	4.0 (4)	0.42
C214	−11201 (3)	−1920 (2)	−5248 (2)	3.3 (2)	F23B	−2472 (15)	−4472 (7)	−3789 (8)	2.4 (3)	0.42
C215	−10473 (3)	−2088 (2)	−4691 (2)	3.1 (2)	F24B	−3308 (17)	−3465 (9)	−3895 (8)	3.2 (4)	0.42
C216	−9672 (3)	−2512 (2)	−4809 (2)	2.6 (2)	F25B	−2272 (21)	−3234 (8)	−5013 (7)	3.6 (4)	0.42
C221	−9200 (3)	−3955 (2)	−6207 (2)	1.7 (1)	F26B	−1515 (13)	−4306 (8)	−4802 (12)	3.3 (4)	0.42
C222	−8870 (3)	−4141 (2)	−6850 (2)	1.7 (1)			Solvent			
C223	−9364 (3)	−4653 (2)	−7250 (2)	2.2 (2)	O4A	−3277 (7)	−5013 (3)	−9662 (4)	1.6 (2)	0.58 (2)
C224	−10190 (3)	−4980 (2)	−7006 (2)	2.6 (2)	O4B	−3953 (12)	−5103 (6)	−9706 (6)	2.8 (3)	0.42
C225	−10520 (3)	−4795 (2)	−6363 (2)	3.3 (2)	CO4A	−4504 (10)	−5059 (6)	−9872 (7)	1.6 (2)	0.58 (2)
C226	−10025 (3)	−4282 (2)	−5963 (2)	2.9 (2)	CO4B	−4724 (17)	−4843 (12)	−9675 (12)	3.9 (5)	0.42
C311	−6909 (3)	−3655 (2)	−7790 (2)	1.7 (1)						

[a] Equivalent isotropic thermal parameters calculated from the anisotropic thermal tensor for atoms with anisotropic thermal parameters. [b] Partial occupancy; where no number is given, pop. = 1.0.

Table V. Selected Bonded and Nonbonded Distances (Å) for $[Co(PP_3)(P(OMe)_3)]BF_4 \cdot 1.5H_2O$

Co–P1	2.211 (6)	P1–C121	1.773 (11)
Co–P2	2.125 (10)	P2–C2	1.91 (2)
Co–P3	2.105 (12)	P3–O1	1.651 (12)
P1–C1	1.91 (2)	O1–CO1	1.47 (2)
P1–C111	1.857 (11)	C1–C2	1.42 (2)

Table VI. Bond Angles (deg) for $[Co(PP_3)(P(OMe)_3)]BF_4 \cdot 1.5H_2O$

P1–Co–P1′	119.3 (2)	P3–O1–CO1	128.8 (13)
P1–Co–P2	85.1 (2)	O1–P3–O1′	102.1 (10)
P1–Co–P3	94.9 (2)	P1–C1–C2	110.4 (15)
P2–Co–P3	180	P1–C111–C112	121.1 (5)
Co–P1–C1	110.6 (7)	P1–C111–C116	118.9 (5)
Co–P1–C111	118.0 (5)	P1–C121–C122	121.2 (5)
Co–P1–C121	122.3 (5)	P1–C121–C126	118.8 (5)
Co–P2–C2	113.6 (7)	P2–C2–C1	110.0 (15)
Co–P3–O1	116.1 (6)		

hydrogen atoms on the coordinated $P(OMe)_3$ were located in the difference electron density map, and the remaining hydrogens were placed at calculated positions (d_{C-H} = 0.95 Å and $B(H) = B_{iso}(C) + 1.0$ Å^2); no hydrogen atoms were included in the refinement for the disordered solvent molecule. The phenyl rings were refined as rigid hexagons (D_{6h} symmetry with d_{C-C} = 1.395 Å). In the final cycles of full-matrix least-squares refinement the nickel, phosphorus, and carbon atoms in the $-CH_2-CH_2-$ chains of the PP_3 ligand, the oxygen atoms of $P(OMe)_3$, and the arsenic atoms were refined anisotropically.

Table VII. Selected Bonded and Nonbonded Distances (Å) for $[Ni(PP_3)(P(OMe)_3)](AsF_6)_2 \cdot MeOH$

Ni–P1	2.275 (2)	P111–C321	1.836 (3)
Ni–P11	2.283 (2)	P2–C2	1.814 (6)
Ni–P111	2.325 (2)	P2–C22	1.813 (6)
Ni–P2	2.181 (2)	P2–C32	1.822 (6)
Ni–P3	2.137 (2)	P3–O1	1.561 (5)
P1–C1	1.832 (6)	P3–O2	1.575 (5)
P1–C111	1.821 (3)	P3–O3	1.562 (4)
P1–C121	1.816 (4)	O1–CO1	1.416 (8)
P11–C21	1.838 (6)	O2–CO2	1.413 (8)
P11–C211	1.822 (3)	O3–CO3	1.445 (8)
P11–C221	1.812 (3)	O4A–CO4A	1.153 (25)
P111–C31	1.833 (6)	O4B–CO4B	1.636 (14)
P111–C311	1.850 (3)		

The final discrepancy indices on F were R = 0.062 and R_w = 0.063 for 7210 reflections with $F_o^2 \geq 3\sigma(F_o^2)$ and 353 variables. The final partial occupancies on each AsF_6^- anion refined to *0.55 (2)* (1 − 0.55 for the other orientation) and 0.58 (4) (1 − 0.58 for the other orientation); respectively, whereas the partial occupancy on the methanol solvent molecule refined to 0.58 (2) (1 − 0.58 for the other orientation). The largest peaks (ca. 1.4 e/Å^3) in the difference electron density map belonged to the methanol solvent molecule. The final values for the atomic parameters are given in Table IV; bond lengths are listed in Tables VII and VIII.

Results and Discussion

Syntheses and Properties of the Complexes. Literature methods[9,13a] were used to prepare the Co(I) and Ni(II) complexes of

Table VIII. Bond Angles (deg) for $[Ni(PP_3)(P(OMe)_3)](AsF_6)_2 \cdot MeOH$

P1-Ni-P11	122.8 (1)	Ni-P111-C31	104.7 (2)
P1-Ni-P111	113.2 (1)	Ni-P111-C311	125.0 (2)
P11-Ni-P111	121.9 (1)	Ni-P111-C321	115.9 (2)
P1-Ni-P2	85.6 (1)	Ni-P2-C2	110.0 (2)
P11-Ni-P2	84.2 (1)	Ni-P2-C22	112.6 (2)
P111-Ni-P2	86.3 (1)	Ni-P2-C32	112.0 (2)
P1-Ni-P3	95.4 (1)	Ni-P3-O1	117.3 (2)
P11-Ni-P3	91.9 (1)	Ni-P3-O2	112.3 (2)
P111-Ni-P3	97.0 (1)	Ni-P3-O3	109.0 (2)
P2-Ni-P3	175.8 (1)	O1-P3-O2	105.1 (3)
Ni-P1-C1	104.8 (2)	O1-P3-O3	103.2 (3)
Ni-P1-C111	125.0 (2)	O2-P3-O3	109.4 (3)
Ni-P1-C121	117.3 (2)	P3-O1-CO1	131.3 (5)
Ni-P11-C21	105.4 (2)	P3-O2-CO2	126.1 (5)
Ni-P11-C211	125.3 (2)	P3-O3-CO3	127.8 (4)
Ni-P11-C221	116.3 (2)		

the tetradentate tripod ligand PP_3 to give compounds with the formulas $[CoL(PP_3)]$ and $[NiL(PP_3)]X$ ($L = Cl^-, Br^-, I^-, CN^-, NCS^-, H^-$; $X = BF_4^-, AsF_6^-$). These compounds are stable in the solid state (except the hydrides), and the solutions are stable when protected from air. In general, the Ni(II) complexes tend to be more stable than the Co(I) complexes. For example, $[NiCl(PP_3)]AsF_6$ is stable for hours in solution, whereas the corresponding $[CoCl(PP_3)]$ is rather unstable in solution.

In the infrared spectra, the $[Co(PP_3)(CO)]^+$ and $[Ni(PP_3)(CO)]^{2+}$ derivatives show a C–O stretching frequency at 1960 and 2070 cm^{-1}, respectively. The corresponding cyanide derivatives show a C–N stretch at 2075 and 2105 cm^{-1}, respectively. The lower C–O and C–N stretching frequencies, which are observed for the Co(I) as compared to the Ni(II) compounds, indicate stronger Co–C bonds in each case. The Co–H stretching frequency of $[CoH(PP_3)] \cdot {}^1/_2(CH_3)_2CO$ is at 1785 cm^{-1}, whereas the Ni–H stretching vibration is at 1885 cm^{-1}; the higher Ni-H absorption indicates that the Ni–H force constant is significantly stronger. The infrared spectrum of $[Co(NCS)(PP_3)]$ shows a broad strong C–N stretching frequency at 2098 cm^{-1}, indicative of a N-bonded thiocyanato ligand.[26]

Several new unreported phosphine and phosphite complexes with the general formulas $[Co(PP_3)(PR_3)]AsF_6$ and $[Ni(PP_3)(PR_3)](AsF_6)_2$ were synthesized in this investigation. The preparative method involves replacement of the halide in the $[CoL(PP_3)]$ and $[NiL(PP_3)]AsF_6$ ($L = Cl^-, Br^-, I^-$) complexes by the appropriate PR_3 ligand (eq 1). The bromide complexes are the

$$[CoBr(PP_3)] + PR_3 + LiAsF_6 \xrightarrow{MeOH} [Co(PP_3)PR_3]AsF_6 + LiBr \quad (1)$$

most convenient starting materials since they undergo substitution more rapidly than the chloro compounds and do not undergo oxidation–reduction reactions as do the iodo complexes. The substitution reactions are accomplished at room temperature for Co(I), whereas refluxing is required for the Ni(II) derivatives. Synthesis of the PR_3 complexes seems to depend on the size of the PR_3 ligand; for example, phosphine complexes containing PR_3 ligands with large cone angles (e.g. PPh_3 and PCy_3) could not be isolated from the reactions on $[CoBr(PP_3)]$. Also, the small phosphite ligands, $P(OR)_3$, could be substituted in the Ni(II)–PP_3 complexes. Another unsuccessful attempt to prepare the PPh_3 complex of $Ni^{II}(PP_3)$ has appeared recently.[2]

The electronic spectra of solutions of the complexes have been used to assign a trigonal-bipyramidal structure to the compounds.[9,11] Typically, low-spin Co(I) and Ni(II) (d^8) complexes show one or two fairly intense bands in the (18–25) $\times 10^3$ cm^{-1} region. These Co(I)–PP_3 complexes displayed one absorption ($\epsilon = \sim 1200$–2100 M^{-1} cm^{-1}) in the 21 $\times 10^3$ cm^{-1} region and a second absorption at approximately 27 $\times 10^3$ cm^{-1} ($\epsilon = \sim 300$); the Ni(II) complexes have only one clearly resolved band at $\sim 22 \times 10^3$ cm^{-1} ($\epsilon = 10\,000$–$14\,000$).

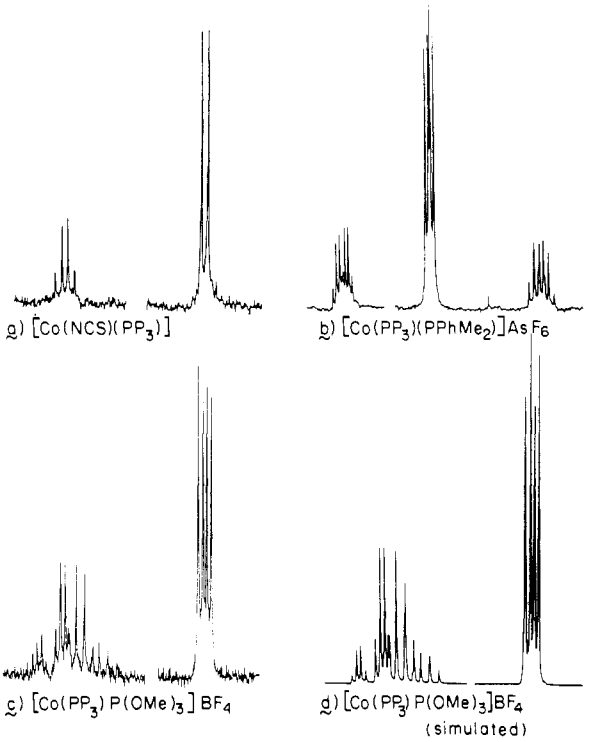

Figure 1. 36.43-MHz $^{31}P\{^1H\}$ NMR spectra of CH_2Cl_2 solutions: (a) $[Co(NCS)(PP_3)]$ at 200 K; (b) $[Co(PP_3)(PPhMe_2)]AsF_6$ at 210 K; (c) $[Co(PP_3)P(OMe)_3]BF_4$ at 190 K. (d) $[Co(PP_3)P(OMe)_3]BF_4$ computer simulated with use of the parameters listed in Table IX.

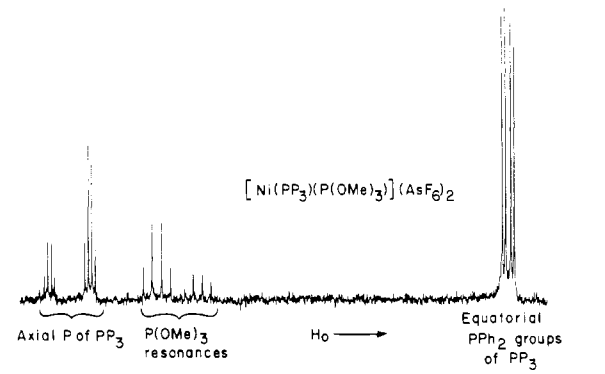

Figure 2. 36.43-MHz $^{31}P\{^1H\}$ NMR spectrum of a CH_2Cl_2 solution of $[Ni(PP_3)P(OMe)_3](AsF_6)_2$ at 300 K.

Phosphorus-31 NMR Spectra. We report here the $^{31}P\{^1H\}$ NMR spectra of the previously synthesized $[CoL(PP_3)]$ and $[NiL(PP_3)]AsF_6$ series of complexes, where L is an anionic ligand, and of the new $[Co(PP_3)(L)]^+$ and $[Ni(PP_3)(L)]^{2+}$ cations, where L is a phosphorus ligand. The $[CoL(PP_3)]$ and $[NiL(PP_3)]^+$ complexes (L = an anionic ligand) have simple first-order AX_3 splitting patterns that produce a quartet for the central bridgehead phosphorus atom (P_2) and a doublet upfield for the terminal PPh_2 groups (P_1) of the tripod ligand PP_3. These ^{31}P NMR spectra are consistent with trigonal-bipyramidal structures, which are demonstrated by electronic spectra of the complexes in solution and by X-ray structural determinations of $[Co(PP_3)P(OMe)_3]BF_4$ and $[Ni(PP_3)P(OMe)_3](AsF_6)_2$ in the solid state. As an illustration of the spectral patterns observed, the $^{31}P\{^1H\}$ NMR spectra of several Co(I) complexes are illustrated in Figure 1 and the $^{31}P\{^1H\}$ NMR spectrum of $[Ni(PP_3)(P(OMe)_3)](AsF_6)_2$ is given in Figure 2.

For those complexes in which a monodentate phosphorus ligand is located trans to the bridgehead atom P_2, more complicated ^{31}P NMR spectra result from coupling with this trans phosphorus atom. The phosphine complexes (L = PEt_3 or $PPhMe_2$) exhibited first-order AMX_3 spin patterns at 36.43 MHz (e.g. Figure 1).

(26) Meek, D. W.; Nicpon, P. E.; Meek, V. I. *J. Am. Chem. Soc.* **1970**, *92*, 5351.

Table IX. Phosphorus-31 NMR Data for the $[CoL(PP_3)]$ and $[Co(PP_3)L]X$ Complexes

compd	chem shifts[a]			coord chem shifts[c]		coupling const, Hz			temp, K
	$\delta(P_1)$	$\delta(P_2)$	$\delta(P_3)$[b]	$\Delta(P_1)$	$\Delta(P_2)$	$^2J_{P_1-P_2}$	$^2J_{P_1-P_3}$	$^2J_{P_2-P_3}$	
$[CoBr(PP_3)]$	49.6	171.9		63.7	190.8	35			200
$[CoI(PP_3)]$	52.7	184.4		66.8	203.3	34			200
$[CoH(PP_3)]\cdot{}^1/_2(CH_3)_2CO$	84.0	183.5		98.1	202.4	18			190
$[CoCN(PP_3)]$	67.2	172.6		81.3	191.5	37			230
$[CoNCS(PP_3)]$	56.1	158.7		70.2	177.6	38			200
$[Co(PP_3)CO]BF_4$	75.9	170.7		90.0	189.6	40			250
$[Co(PP_3)(PPhMe_2)]AsF_6$	53.3	152.3	18.0	67.4	171.2	40	59	104	210
$[Co(PP_3)(PEt_3)]AsF_6$	52.9	147.2	29.9	67.0	166.1	37	57	98	250
$[Co(PP_3)(P(OMe)_3)]BF_4$	68.5	168.7	159.7	82.6	187.6	39	86	227	190
$[Co(PP_3)(PPh_2OMe)]AsF_6$	63.8	159.9	155.9	77.9	178.8	43	57	146	190
$[Co(PP_3)(PMe(O\text{-}i\text{-}Pr)_2]AsF_6$	58.2	152.9	192.8	72.3	171.8	40	75	176	190
$[Co(PP_3)(PF_2OMe)]AsF_6$[d]	67.2	162.1	176.7	81.3	181.0	46	85	232	190

[a] The chemical shift values (δ's) are relative to 85% H_3PO_4, with positive values being downfield from the standard. [b] P_1 is the designation for the PPh_2 groups, and P_2 is the central P of PP_3; P_3 is the phosphorus atom of a monodentate PR_3 or $P(OR)_3$ ligand. [c] $\delta(P_1) = -14.1$, $\delta(P_2) = -18.9$, and $^2J_{P_1-P_2} = 24$ Hz for the free ligand PP_3. [d] $^3J_{P_1-F} = 15$ Hz, $^3J_{P_2-F} = 16$ Hz, $^1J_{P_3-F} = 1190$ Hz.

Table X. Phosphorus-31 NMR Data for the $[NiL(PP_3)]X$ and $[Ni(PP_3)L]X_2$ Complexes

compd	chem shifts[a]			coord chem shifts[c]		coupling const, Hz			temp, K
	$\delta(P_1)$	$\delta(P_2)$	$\delta(P_3)$[b]	$\Delta(P_1)$	$\Delta(P_2)$	$^2J_{P_1-P_2}$	$^2J_{P_1-P_3}$	$^2J_{P_2-P_3}$	
$[NiCl(PP_3)]AsF_6$	32.4	140.9		46.5	159.8	28			200
$[NiBr(PP_3)]AsF_6$	34.0	151.9		48.1	170.8	26			240
$[NiI(PP_3)]AsF_6$	38.2	167.1		52.3	186.0	22			240
$[NiH(PP_3)]AsF_6$	62.5	160.4		76.6	179.3	17			210
$[NiCN(PP_3)]AsF_6$	47.8	155.2		61.9	174.1	31			240
$[Ni(PP_3)CO](BF_4)_2$	64.5	178.6		78.6	197.5	21			200
$[Ni(PP_3)P(OMe)_3](AsF_6)_2$	43.7	147.5	123.8	57.8	166.4	28	78	353	300
$[Ni(PP_3)P(OEt)_3](AsF_6)_2$	41.5	142.8	119.2	55.6	161.7	30	78	348	300
$[Ni(PP_3)P(OCH_2CF_3)_3](BF_4)_2$	42.9	151.2	132.4	57.0	170.1	29	77	338	300

[a] The chemical shift values (δ's) are relative to 85% H_3PO_4, with positive values being downfield from the standard. [b] P_1 is the designation for the PPh_2 groups and P_2 is the central P of PP_3; P_3 is the phosphorus atom of a monodentate PR_3 group or $P(OR)_3$ ligand. [c] $\delta(P_1) = -14.1$, $\delta(P_2) = -18.9$, and $^2J_{P_1-P_2} = 24$ Hz for the free ligand PP_3.

Table XI. Effect of the Trans Ligand on the Chemical Shift of the Bridgehead Phosphorus: Trans Influence on $\Delta(P_2)$ (Hz)[a]

$[Co(PP_3)L]^{n+}$ series	I^-	<	H^-	<	CN^-	<	Br^-	<	CO	<	$P(OMe)_3$	<	PF_2OMe	<	PPh_2OMe	<	$-NCS^-$	<	$PPhMe_2$	<	PEt_3
$\Delta(P_2)$	203.3		202.4		191.5		190.8		189.6		187.6		181.0		178.8		177.6		171.2		166.1

$[Ni(PP_3)L]^{n+}$ series	CO	<	I^-	<	H^-	<	CN^-	<	Br^-	<	$P(OCH_2CF_3)_3$	<	$P(OMe)_3$	<	$P(OEt)_3$	<	Cl^-
$\Delta(P_2)$	197.5		186.0		179.3		174.1		170.8		170.1		166.4		161.7		159.8

[a] $n = 0$, 1 for the anionic and neutral ligands L, respectively, in the cobalt series, whereas $n = 1$, 2 for the nickel series.

When the trans phosphorus ligand has a chemical shift close (L = phosphite) to that of the P_2 bridgehead, second-order ABX_3 splitting patterns are obtained (e.g., Figure 1c). A computer-simulated spectrum is given in Figure 1d for comparison. The spectrum of $[Ni(PP_3)(P(OMe)_3)](AsF_6)_2$, which is shown in Figure 2, is a second-order ABX_3 splitting pattern.

The ^{31}P NMR resonance of a phosphorus ligand shifts (usually downfield) from the position of the free ligand when it becomes bonded to a metal atom; this shift is treated quantitatively as the coordination chemical shift, Δ, which is defined as $\delta(P_{coordinated}) - \delta(P_{free\ ligand})$.[27,28] In addition, if a phosphorus atom is incorporated into a chelate ring, a significant additional contribution to the chemical shift, designated Δ_R, is observed.[29] Phosphorus atoms in five-membered rings display unusually large downfield Δ_R contributions. Earlier, we noted that if a phosphorus atom is located at the bridgehead of two or three five-membered rings, the large downfield shift is exaggerated,[30] the downfield shift being nearly additive for each chelate ring. When the PP_3 ligand is chelated to a metal ion, both P_2 and P_1 donor groups are subject to the five-membered ring effect; however, the coordination chemical shift of the apical phosphorus atom (P_2) is exceptionally large, since it is common to three five-membered chelate rings.[13b] The coordination chemical shift $\Delta(P_2)$ is in the range 160-200 ppm, depending on the trans ligand. The PPh_2 groups (P_1), which are involved in one chelate ring, show $\Delta(P_1)$ values in the range 50–100 ppm. The difference between the coordination chemical shifts of the axial phosphorus $\Delta(P_2)$ and the equatorial phosphorus atoms $\Delta(P_1)$ is relatively constant at approximately 100 ppm for most of the complexes. The ^{31}P NMR data for the Co(I) and Ni(II) complexes are summarized in Tables IX and X.

Both chemical shifts $\delta(P_1)$ and $\delta(P_2)$ are sensitive to variation of the trans ligand L. Phosphines (e.g., PEt_3 and $PPhMe_2$) exert the largest influence on the ^{31}P resonances of the P_2 phosphorus atom, causing it to shift to a higher field. The δP_2 values of the halide complexes occur at lower fields, indicating that the electronegative halogen ligands exert a deshielding effect. A large coordination chemical shift $\Delta(P_2)$ indicates a small trans influence by the fifth ligand. Thus, on the basis of the $\Delta(P_2)$ values, the trans influence of the fifth ligand in these complexes is $PR_3 > P(OR)_3 > X^-$.

The effect of the trans ligand on the chemical shift of the apical P_2 phosphorus for both the Co(I) and Ni(II) series of complexes

(27) Grim, S. O.; Barth, R. C; Mitchell, J. D.; Del Gaudio, J. *Inorg. Chem.* **1977**, *16*, 1776.
(28) Grim, S. O.; Briggs, W. L.; Barth, R. C.; Tolman, C. A; Jesson, J. P. *Inorg. Chem.* **1974**, *13*, 1095.
(29) (a) Garrou, P. E. *Inorg. Chem.* **1975**, *14*, 1435. (b) Garrou, P. E. *Chem. Rev.* **1981**, *81*, 229.
(30) Meek, D. W.; Mazanec, T. J. *Acc. Chem. Res.* **1981**, *14*, 266.

is $PEt_3 > PPhMe_2 > PPh_2OMe > Cl^- > P(OMe)_3 > Br^- > CN^- > H^- > I^-$ (Table XI). For the halides, the order of trans influence is $Cl^- > Br^- > I^-$ according to $\Delta(P_2)$ which appears to be opposite to the order expected on the basis of the halide electronegativities. The fact that $\delta(P_1)$ also changes with variation of L indicates that there is a cis influence in the ^{31}P NMR spectra of these compounds, as well as a trans influence. For the iodide and bromide complexes the difference between $\Delta(P_2)$ and $\Delta(P_1)$ (approximately 135 ppm for I^- and 125 ppm for Br^-) is larger than for the other complexes. The larger difference indicates a larger cis influence (shielding) on the equatorial phosphorus atoms (P_1) and/or a smaller trans influence on the axial P_2 by I^- and Br^-. A large cis influence could cause a reversal in the $\Delta(P_2)$ trends.

The cavity for the fifth ligand in these trigonal-bipyramidal PP_3 complexes should be relatively small because of the steric requirements of the six phenyl groups on the terminal PPh_2 groups. Therefore, I^- and Br^- ligands should have a larger steric effect than Cl^-; analogously, the phosphines used here have a larger cone angle[31] than the phosphites. In addition, the PPh_2 groups of PP_3 are oriented so that π-interaction between a phenyl ring of each PPh_2 group and the fifth ligand could occur, thereby giving rise to a cis influence by the fifth ligand.

For the halide complexes the $^2J_{P_1-P_2}$ coupling constants increase in the order $I^- < Br^- < Cl^-$, whereas both $\delta(P_1)$ and $\delta(P_2)$ increase (downfield shift) in the opposite order, i.e., $Cl^- < Br^- < I^-$. The reversed order of P–P coupling constants and chemical shifts had been observed in other complexes.[32]

On the basis of its strong trans influence in planar and octahedral complexes,[33] one could have expected the ^{31}P resonances of P_2 in the $[CoH(PP_3)]$ and $[NiH(PP_3)]^+$ complexes to occur in the region of 130–135 ppm. However, the actual $\delta(^{31}P)$ values are farther downfield, indicating that the hydride ligands exerts a relatively small influence on both the cis and trans phosphorus atoms in these trigonal-bipyramidal complexes. This effect may be explained by a relatively weak M–H bond, which is consistent with the low ν_{Co-H} and ν_{Ni-H} stretching frequencies. The phosphorus–phosphorus coupling constants for the Co–H and Ni–H complexes of PP_3 are also anomalously small, as compared to the other Co(I) and Ni(II) values in Tables IX and X. Note that, except for H^-, the $^2J_{P_1-P_2}$ values are fairly constant, particularly for the Co(I) series.

The ^{31}P NMR chemical shifts and the infrared ν_{CO} values indicate that the trans influence of CO is significantly different in the $[Co(PP_3)CO]^+$ and $[Ni(PP_3)CO)]^{2+}$ complexes. The $\Delta(P_2)$ value for $[Ni(PP_3)CO](AsF_6)_2$ is the largest (the trans influence is smallest) of all the Ni(II) complexes studied here. The single C–O stretching frequencies of the Co(I) and Ni(II) carbonyl complexes occur at 1960 and 2070 cm^{-1}, respectively. These infrared data suggest that Co–C interaction is stronger than the Ni–C bonding, which is consistent with the general observation that CO complexes of Ni(II) are less stable than the corresponding CO complexes of Co(I).

When the $\delta(P_2)$ values for the $[Ni(PP_3)P(OEt)_3](AsF_6)_2$ and $[Ni(PP_3)P(OCH_2CF_3)_3](BF_4)_2$ complexes are compared, $\delta(P_2)$ for the $P(OCH_2CF_3)_3$ derivative is farther downfield, which is consistent with the deshielding effect of the electronegative OCH_2CF_3 groups of the $P(OCH_2CF_3)_3$ ligand.

Phosphorus–phosphorus coupling for the $[Co(PP_3)(PR_3)]X$ complexes are given in Table IX. Both the trans P–P ($^2J_{P_2-P_3}$) and cis P–P ($^2J_{P_1-P_3}$) coupling constants are larger for the phosphite complexes than for the phosphine complexes (i.e., $(RO)_3P > R_3P$) since increasing electronegativity of the substituent on phosphorus increases the s character of the phosphorus lone pair. These P–P coupling constants are consistent with those reported for other trigonal-bipyramidal polyphosphine Co(I) complexes.[34] The range of trans P–P coupling constants ($^2J_{P_2-P_3}$) for phosphine–phosphine

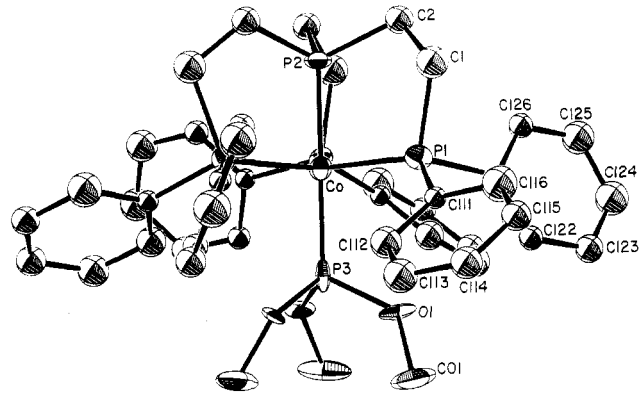

Figure 3. Perspective view of the cation $[Co(PP_3)P(OMe)_3]^+$ (**1**) without the hydrogen atoms.

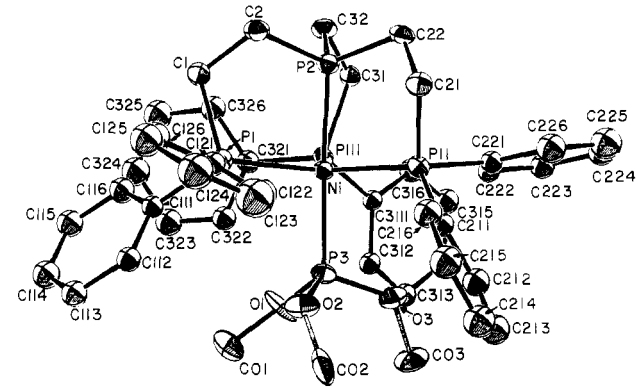

Figure 4. Perspective view of the cation $[Ni(PP_3)P(OMe)_3]^{2+}$ (**2**) without the hydrogen atoms.

coupling is 98–104 Hz, and the cis range ($^2J_{P_1-P_3}$) is 57–59 Hz in these $[Co(PP_3)PR_3]X$ complexes. The analogous $^2J_{P_2-P_3}$ value for phosphine–phosphite coupling in $[Co(PP_3)P(OMe)_3]AsF_6$ is 227 Hz, while $^2J_{P_1-P_3}$ is 86 Hz.

As expected, the coupling constants of the PPh_2OMe complex more closely resemble those for a phosphine ligand ($^2J_{P_1-P_3}$ = 57 Hz and $^2J_{P_2-P_3}$ = 146 Hz), whereas the coupling constants for the $PMe(O\text{-}i\text{-}Pr)_2$ complex are more like those for a phosphite ligand ($^2J_{P_1-P_3}$ = 75 Hz and $^2J_{P_2-P_3}$ = 176 Hz).

The coupling constant data for $[Ni(PP_3)P(OMe)_3](AsF_6)_2$ are given in Table X. The $\delta(P_3)$ value of $P(OMe)_3$ in the Ni(II) complex is shifted upfield compared to that in the Co(I) complex, and the trans coupling constant $^2J_{P_2-P_3}$ is significantly larger (353 Hz vs. 227 Hz).

Structures of $[Co(PP_3)P(OMe)_3]BF_4 \cdot 1.5H_2O$ and $[Ni(PP_3)P(OMe)_3](AsF_6)_2 \cdot MeOH$. The $[Co(PP_3)(P(OMe)_3)]^+$ cation (**1**) lies on the crystallographic 3-fold axis and is a slightly distorted trigonal bipyramid (Figure 3). Likewise, $[Ni(PP_3)(P(OMe)_3)]^{2+}$ (**2**), shown in Figure 4, is a slightly distorted trigonal bipyramid; however, the nickel complex is distorted from ideal C_3 symmetry in the crystal. The metal atoms in **1** and **2** lie 0.12 Å below the equatorial plane of the trigonal bipyramid toward the trimethyl phosphite ligand. Whereas ideal C_3 symmetry is maintained in the crystal by **1**, the three equatorial phosphorus atoms (P1, P11, P111) of **2** are crystallographically nonequivalent. The equatorial Ni–P111 distance, 2.325 (2) Å, is longer than the other two equatorial distances, Ni–P1 = 2.275 (2) Å and Ni–P11 = 2.283 (2) Å.

Since the P1–Ni–P11 equatorial angle, 122.8 (1)°, opposite the Ni–P111 bond has not opened as much as commonly occurs in other distorted trigonal-bipyramidal structures such as $[NiCl(np_3)]PF_6$, $np_3 = N(CH_2CH_2PPh_2)_3$,[35] the distortion in this PP_3 structure appears to be due to packing forces. In the np_3 complex one equatorial Ni–P distance is 2.298 (4) Å vs. 2.194

(31) Tolman, C. A. *Chem. Rev.* **1977**, *77*, 313.
(32) Verkade, J. G. *Coord. Chem. Rev.* **1972/1973**, *9*, 1.
(33) Moore, D. S.; Robinson, S. D. *Chem. Soc. Rev.* **1983**, *12*, 415.
(34) Dubois, D. L; Meek, D. W. *Inorg. Chem.* **1976**, *15*, 3076.
(35) Di Vaira, M.; Sacconi, L. *J. Chem. Soc., Dalton Trans.* **1975**, 493.

(5) and 2.223 (4) Å for the other two equatorial Ni-P distances; the equatorial P-Ni-P angles opposite the equatorial bonds are 126.7 (2), 118.8 (2), and 114.0 (2)°, respectively. In the case of $[Ni(PP_3)P(OMe)_3]^{2+}$, the distortion from ideal C_3 symmetry may result from one AsF_6^- counterion contacting with the phenyl substituents on the P111 atom, where the C···F distance is ca. 3.1 Å. The closest intramolecular contacts in **1** and **2** are between the $P(OMe)_3$ ligand oxygen atoms and the phenyl substituents on the PP_3 ligand, O···C distances ca. 3.2 Å.

As a result of the smaller covalent radius of a phosphite phosphorus atom, metal-phosphite M-P distances are generally shorter than metal-phosphine distances. The same trend is observed in these two structures. In both **1** and **2** the shortest metal-ligand distances are the metal-phosphite distances (2.105 (12) and 2.137 (2) Å, respectively). The next shortest metal-phosphorus distance in **1** and **2** is to the apical phosphorus atom, P2 (2.125 (10) and 2.182 (2) Å, respectively). The nickel to equatorial phosphorus distance, 2.294 (2) Å average, in **2** not only is the longest metal-phosphorus distance in **1** and **2** but also is unexpectedly longer than the cobalt to equatorial phosphorus distance, 2.211 (6) Å, in **1**. The Co-phosphite distance, 2.105 (12) Å, in **1** is significantly shorter than the apical and equatorial Co-phosphite distances (2.141 (5) and 2.150 (5) Å, respectively) in the distorted trigonal-bipyramidal complex $[Co(etp)(P(OMe)_3)_2]BF_4$ (etp = $PhP(CH_2CH_2PPh_2)_2$).[36] The apical and equatorial Co-phosphine distances in $[Co(etp)(P(OMe)_3)_2]BF_4$ are comparable to the Co-phosphine distances observed in this study.

Approximate cone angles measured for the trimethyl phosphite ligand in **1** and **2** are 87 and 94°, respectively (cf., Tolman cone angle of 107° for the ligand $P(OMe)_3$).[31] The 7° difference in the trimethyl phosphite cone angle between **1** and **2** is manifested in the M-P-O and O-P-O angles. The Co-P-O angle in **1** is ca. 3° larger than the average Ni-P-O angle in **2**. The O-P-O angle in **1** is ca. 4° smaller than the average O-P-O angle in **2**. The O-P and O-C distances and P-O-C angles of the trimethyl phosphite are relatively insensitive to the difference in the trimethyl phosphite cone angle between **1** and **2**. The 7° difference between the cone angle of $P(OMe)_3$ in **1** and **2** may be due to the shorter Co-$P(OMe)_3$ and Co-P_{eq} distances vs. longer Ni-$P(OMe)_3$ and Ni-P_{eq} distances. The shorter Co-P_{eq} bond lengths, ca. 0.06-0.11 Å shorter, result in the phenyl substituents on the equatorial phosphorus atoms being held closer to the Co-$P(OMe)_3$ coordination site than for the corresponding Ni-$P(OMe)_3$ coordination site. The $P(OMe)_3$ ligand is sufficiently flexible to accommodate changes in its internal geometry at the M-P-O and O-P-O angles, and it exhibits the common head-to-tail conformation found in other transition-metal complexes of trimethyl phosphite.[37] Curiously, the trimethyl phosphite ligand in **1** is coordinated in a sterically more demanding eclipsed conformation relative to the PP_3 ligand, and it appears to rotate in the same direction as the PP_3. The trimethyl phosphite in **2** is coordinated in a less sterically demanding gauche conformation and appears to turn in the opposite direction from the PP_3 ligand. Otherwise, the geometrical features of trimethyl phosphite in **1** and **2** are similar to those previously reported.[37]

Acknowledgment. The authors express appreciation to Loren Chen for assitance in obtaining some of the $^{31}P\{^1H\}$ NMR spectra, to Dr. Judith Gallucci for technical advice on the X-ray studies, to Dr. Steven Socol for helpful comments on this manuscript, and to Marietta College for a sabbatical leave to W.H.H. The research was partially supported by the University Exploratory Research Program of the Procter and Gamble Co.

Registry No. **1**, 99687-47-5; **2**, 99687-50-0; $[Co(PP_3)(PPh_2OMe)]AsF_6$, 99687-52-2; $[Co(PP_3)(PEt_3)]AsF_6$, 99687-54-4; $[Co(PP_3)(PPh_2Me)]AsF_6$, 99705-72-3; $[Ni(PP_3)(P(OEt)_3)](AsF_6)_2$, 99687-56-6; $[Ni(PP_3)(P(OCH_2CF_3)_3)](BF_4)_2$, 99687-58-8; $[Co(PP_3)CO]BF_4$, 99687-59-9; $CoCl(PP_3)$, 55297-75-1; $CoBr(PP_3)$, 55236-46-9; $CoI(PP_3)$, 55236-47-0; $Co(CN)(PP_3)$, 55236-49-2; $Co(NCS)(PP_3)$, 55236-48-1; $[Co(P(OMe)_3)_5]BF_4$, 99687-60-2; $[NiCl(PP_3)]AsF_6$, 99687-61-3; $[NiBr(PP_3)]AsF_6$, 99687-63-5; $[NiI(PP_3)]AsF_6$, 99687-65-7; $[NiH(PP_3)]AsF_6$, 99705-73-4; $[Ni(PP_3)CO](BF_4)_2$, 99687-67-9; $[Co(PP_3)(PMe(O\text{-}i\text{-}Pr)_2)]AsF_6$, 99687-69-1; $[Co(PP_3)(PF_2OMe)]AsF_6$, 99687-71-5; $[Ni(PP_3)CN]^+$, 99687-72-6; $CoH(PP_3)$, 55088-11-4.

Supplementary Material Available: Tables of hydrogen positional parameters, anisotropic thermal parameters, and observed and calculated structure factor amplitudes (42 pages). Ordering information is given on any current masthead page.

(36) Dubois, D. L.; Mason, R.; Meek, D. W.; Scollary, G. R. *J. Organomet. Chem.* **1976**, *114*, C30.

(37) Jacobson, R. A.; Karcher, B. A.; Montag, R. A.; Socol, S. M.; Vande Griend, L. J.; Verkade, J. G. *Phosphorus Sulfur* **1981**, *11*, 27 and references cited therein.

Contribution from the Laboratoire d'Etude des Solutions Organiques et Colloidales, UA CNRS 406, Université de Nancy I, 54506 Vandoeuvre-les-Nancy Cedex, France

Carbon-13 and Proton Relaxation in Paramagnetic Complexes of Amino Acids. Structure and Dynamics of Copper(II)-L-Histidine (1:2) in Aqueous Solution

Bernard Henry, Jean-Claude Boubel, and Jean-Jacques Delpuech*

Received March 25, 1985

The ^{13}C relaxation times T_1 and T_2 and the isotropic shifts of 0.95 M aqueous solutions of L-histidine at pH 10.5 (or pD 10.9) containing ca. 10^{-3} M copper(II) perchlorate are measured at 62.86 MHz over a temperature range of 20-70 °C. T_1 is shown to be purely dipolar and controlled by the tumbling rate of the complex, while T_2 is purely scalar and controlled by both ligand exchange and electronic relaxation. This allows us to extract carbon-to-metal distances, using the known geometry of the imidazole ring and hyperfine coupling constants: A_C = 1.60, -1.65, 0.37, 0.92, and 2.05 MHz for C_1, C_2, C_3, C_4, and C_6, respectively. Dynamic parameters were preferably extracted from the ^1H NMR of proton H_6 at 250 MHz, yielding the tumbling correlation time τ_R(25 °C) = 1.25×10^{-10} s, the L-histidine exchange rate k_M(25 °C) = 7.46×10^5 s^{-1} (and the corresponding activation parameters, $\Delta H^* = 9.4$ kcal mol^{-1} and $\Delta S^* = 0.0$ eu), and the electronic relaxation time $T_{1e} = 0.92 \times 10^{-9}$ s. The structure of the complex in solution most likely involves two tridentate histidine molecules. The T_{1e} value is shown to be in reasonable agreement with the one computed from ESR data and the above τ_R value, showing the predominant contribution of spin-rotation interaction compared to the effect of **g** and **A** tensor anisotropy.

Introduction

Copper complexes play an essential role in biochemistry and pharmacology. Certain copper(II)-protein complexes serve as enzymes required by all cells in the human body for normal metabolic processes.[1] Transport of copper(II) in blood is vital to maintaining its concentration at a constant level. It has been shown that copper(II) was bound under physiological conditions

(1) Frieden, E. In "Metal Ions in Biological Systems"; Sigel, H., Ed.; Marcel Dekker: New York, 1981; Vol. 13, Chapter 1.

0020-1669/86/1325-0623$01.50/0